Numerical study of the nanocomposite phase change material-based heat sink for passive cooling of electronic components.

Adeel Arshad[a], Mark Jabbal[a], Hamza Faraji[b], Pouyan Talebizadehsardari[c,d], Muhammad Anser Bashir[e], Yuying Yan[a,f,*]

[a]*Fluids & Thermal Engineering (FLUTE) Research Group, Faculty of Engineering, University of Nottingham, Nottingham NG7 2RD, UK*
[b]*Physics Department, LPMMAT Laboratory, Faculty of Sciences Ain Chock, Hassan II University, Casablanca, Morocco*
[c]*Metamaterials for Mechanical, Biomechanical and Multiphysical Applications Research Group, Ton Duc Thang University, Ho Chi Minh City, Vietnam*
[d]*Faculty of Applied Sciences, Ton Duc Thang University, Ho Chi Minh City, Vietnam*
[e]*Department of Mechanical Engineering, Mirpur University of Science & Technology (MUST), Mirpur 10250, AJK, Pakistan*
[f]*Research Centre for Fluids and Thermal Engineering, University of Nottingham Ningbo China, Ningbo 315100, China*

Abstract

The current two-dimensional (2D) numerical study presents the melting phenomenon and heat transfer performance of the nanocomposite phase change material (NCPCM) based heat sink. Metallic nanoparticles (copper: Cu) of different volume fractions of 0.00, 0.01, 0.03, and 0.05 were dispersed in RT–28HC, used as a PCM. Transient simulations with conjugate heat transfer and melting/solidification schemes were formulated using finite–volume–method (FVM). The thermal performance and melting process of the NCPCM filled heat sink were evaluated through melting time, heat storage capacity, heat storage density, rate of heat transfer and rate of heat transfer density. The results showed that with the addition of Cu nanoparticles, the rate of heat transfer was increased and melting time was reduced. The reduction in melting time was obtained of −1.36%, −1.81%, and −2.56% at 0.01, 0.03, and 0.05, respectively, compared with 0.00 NCPCM based heat sink. The higher heat storage capacity enhancement of 1.87% and lower reduction of −7.23% in heat storage density was obtained with 0.01 volume fraction. The enhancement in rate of heat transfer was obtained of 2.86%, 2.19% and 1.63%; and reduction in rate of heat transfer density was obtained of −6.33%, −21.05% and −31.82% with 0.01, 0.03, and 0.05 volume fraction of Cu nanoparticles, respectively. The results suggest that Cu nanoparticles of 0.01

*Correspondence authors
Email address: yuying.yan@nottingham.ac.uk (Yuying Yan)

volume fraction has the lower melting rate, higher heat storage capacity and heat transfer rate, lower heat storage density and heat transfer rate density which is preferable for passive cooling electronic components.
Keywords: Nanocomposite phase change material; Copper nanoparticles; Heat sink; Electronics cooling

---

Nomenclature

Abbreviations

Al_2O_3	Aluminum oxide
Cu	Copper
FVM	Finite volume method
HS	Heat sink
ICs	Integrated circuits
NCPCM	Nanocomposite phase change material
PCM	Phase change material
PRESTO	PREssure STaggering Option
QUICK	Quadratic Upstream Interpolation for Convective Kinematics
SIMPLE	Semi-Implicit Pressure-Linked Equation
UDF	User–defined function

Symbols

A_m	Mushy zone
B	Boltzman constant (J/K)
ρc_p	Volumetric heat capacity ($J/m^3.K$)
f_l	Liquid fraction
g	Gravitational acceleration (m/s^2)
H	Height (mm)
Q	Heat storage capacity (J)
q	heat storage density (J/kg)
k	Thermal conductivity ($W/m.K$)
L	Latent heat of fusion ($J/kg.K$)
m	Mass (Kg)
p	Pressure (Pa)
$\dot{Q}$	Rate of heat transfer (W)
$\dot{q}$	Rate of heat transfer density (W/kg)
S	Source term in momentum equation
T	Temperature (K)
t	Time (sec)
u	Velocity component in $x-$axis (m/s)
v	Velocity component in $y-$axis (m/s)
W	Width (mm)
c_p	Specific heat capacity ($J/kg.K$)
ΔH	Fractional latent-heat ($J/kg.K$)
$2D$	Two dimensional

Greek letters

φ	Volume fraction
μ	Viscosity (Pa.s)
β	Thermal expansion coefficient (1/K)

Subscripts

HS	Heat sink
hs	Heat source
ini	Initial
l	Liquidus
m	Melting
$ncpcm$	Nanocomposite phase change material
np	Nanoparticles
ref	Reference
x	$x-$axis
y	$y-$axis

1. Introduction

The recent advancement of technology in electronics industries and communication has led to the miniaturization and more power for electronic chips. As a result of this, the operating temperature has been recognized as critical factor which deteriorates the performance and efficiency of integrated circuits (ICs) [1]. Therefore, the design and cooling performance of cooling devices are crucial to remove the excessive heat flux. An effective and efficient thermal management has become vital to maintain or lower the electronic components temperature lower then their maximum allowable operating temperature to increase the lifespan and reliability of electronic components and to avoid the major breakdown [2].

Passive cooling technology of electronics presents an efficient and clean technology with zero emission energy, when it is integrated to a phase–change phenomenon. Phase change materials (PCMs) can be widely used in heat sinks for practical electronic cooling applications due to high storage capacity and providing an almost constant temperature on the surface of the electronic device during the phase change process. In addition to the electronic cooling, due to the advantages of latent heat storage compared with sensible heat storage, PCMs has been widely engaged with space heating [3], photovoltaic panel cooling [4], waste heat recovery [5], low temperature district heating [6, 7], ground source heat pumps integration [8], etc. Solid–liquid phase–change process exhibits by the PCM absorb the heat rejected by electronic device when integrated with a heat sink at constant and intermittent heat fluxes [9, 10]. Due to the intrinsic lower thermal conductivity of PCM causes to delay the heat dissipation rate from electronic devices. Therefore, to enhance the thermal conductivity of PCM, nanoparticles of higher thermal conductivity is dispersed in PCM to improve the heat transfer rate [11, 12]. Several studies have been reported based on nanoparticles enhanced PCM for thermal energy storage [13, 14]. Lin and Al-Kayiem [15, 16] examined the thermophysical properties of Cu nanoparticles dispersed in paraffin wax of various weight percentages. The authors found that by adding the Cu nanoparticles, the thermal conductivity was increased and melting temperature and latent-heat of fusion were reduced. The enhancement in thermal conductivity was reported of 14.0%, 23.9%, 42.5% and 46.3% by adding 0.5%, 1.0%, 1.5% and 2.0% weight percentages of Cu nanoparticles. Colla et al. [17] studied the thermophysical and heat transfer performance of nano-PCM in a square cavity. The results showed that nano-PCM delayed the melting process compare to the pure PCM. Bondareva et al. [18] investigated the heat transfer performance of NCPCM filled cooling system and found the increase in melting rate with increase of nanoparticles concentration. Authors reported that melting phenomenon accelerated by adding nanoparticles initially due to heat conduction in solid and liquid PCM layers. Further, the authors investigated the 2D numerical study to formulate the melting process of paraffin enhanced with Al_2O_3 nanoparticles in a heat sink oriented at different angles [19]. Authors carried out the distribution of velocity and temperature as a function of time and concentration of nanoparticles. It was found that adding nanoparticles accelerated the heat exchange within the system and reduced the melting time of PCM at any inclination angle. More further, authors reported that optimal volume fraction of nanoparticles was the function of volumetric heat generation and fins height. Mahdi and Nsofor [20] proposed a numerical study on solidification process of Al_2O_3 nanoparticles based NCPCM inside a triplex–tube thermal energy storage system. The volume concentration of nanoparticles was varied from $0-8\%$ and solidification time was reduced from 8% to 20% with 3% and 8% loading of Al_2O_3 nanoparticles. Moreover, it was found that with the addition of nanoparticles did not show the significant change in solidification process. However, as time elapsed and loading was increase, the rate of solidification was increased. Ebrahimi and Dadvand [21] studied numerically the melting process of NCPCM by using Al_2O_3 nanoparticles in a rectangular enclosure by using four different arrangements of heat source. The effect of different nanoparticles volume fraction was analysed. The results showed that the loading content of 2% Al_2O_3 nanoparticles had the highest melting rate and better heat transfer rate. Hosseinizadeh et al. [22] numerically investigated the melting of NCPCM using RT–27 and copper nanoparticles in a spherical container. Three different concentrations of nanoparticles were changed and results were obtained that increasing the concentration of copper nanoparticles increased the effective thermal conductivity and lowered the latent–heat of fusion. Arshad et al. [23, 24, 25, 26] conducted the numerical and experimental studies to explore the fin thickness of finned heat sink at constant volume fraction of 9% by different PCMs, volumetric fractions of PCM and different power levels. The results reported that 3 mm fin thickness had the better thermal performance by lowering the average heat sink temperature. Recently, Faraji et al. [27, 28] reported the results of a numerical study of the natural convection induced by NCPCM melting in a inclined rectangular enclosure. The objective of the study was to reveal the effect of the insertion of metallic nanoparticles by quantifying their contribution to the overall thermal response of the heat sink. The results showed that the addition of nanoparticles contributes to efficient cooling of the electronic component by decreasing the average operating temperature.

The present study explore the thermal performance and melting phenomenon of NCPCM based heat sink by using copper (Cu) nanoparticles of four different volume fractions of 0.00, 0.01, 0.03, and 0.05 dispersed in RT–28HC, used as a PCM, at a constant power level of 5 W applied at heat sink base. The key novelty of the current study is to study the heat flow and melting interface of NCPCM filled in heat sink specially used for portable electronic devices which has been rarely discussed in the literature. The transient simulations are carried out through control volume approach to study the solid-liquid phase field, heat flow field and temperature variations. The thermal enhancement performance of the NCPCM filled heat sink is evaluated through different thermal performance evaluation indicators such melting time, heat storage capacity, heat storage density, rate of heat transfer, and rate of heat transfer density for the solution of efficient passive cooling of electronic components.

2. Geometric and Mathematical description

2.1. Physical model

The cross-sectional isometric view of a three-dimensional heat sink filled with NCPCM and other components, used for passive cooling of electronics devices, is shown in 1a which has been employed in previous experimental studies by Arshad et al. [24, 25, 26]. The physical domain of the NCPCM based heat sink considered in current study is shown in Figure 1b. Since the heat flow is symmetrical along the axis, thus two-dimensional (2D) heat flow simulations are carried out. A 2D rectangular heat sink with width (W = 70 mm) and height (H = 25 mm) is heated with a heat source of volumetric heat generation ($q^{'''}$) with sizes of l = 50 mm and t = 2 mm. All the sides of heat sink are adiabatic except top surface which undergoes with natural convection. The internal cavity of the heat sink having width (w = 60 mm) and height (h = 20 mm) is filled with different volume fractions (φ = 0.00, 0.01, 0.03, and 0.05) of nanoparticles. The heat sink made of copper is numerically modelled to investigate the thermal performance and melting phenomenon of NCPCM at a constant power input of 5 W. The thermophysical properties of RT–28HC which is used PCM and copper (Cu) nanoparticles are listed in Table 1. The current system is designed to investigate passive thermal performance NCPCM based heat sink of portable electronic components.

2.2. Numerical model

The numerical model is developed based the physical domain presented in the Figure 1. The conduction heat transfer mode is considered for the heat sink while conduction and convection heat transfer are considered for NCPCM (mixture of PCM and nanoparticles). Following assumptions are the necessary taken to model the NCPCM based heat sink problem presented in this work:

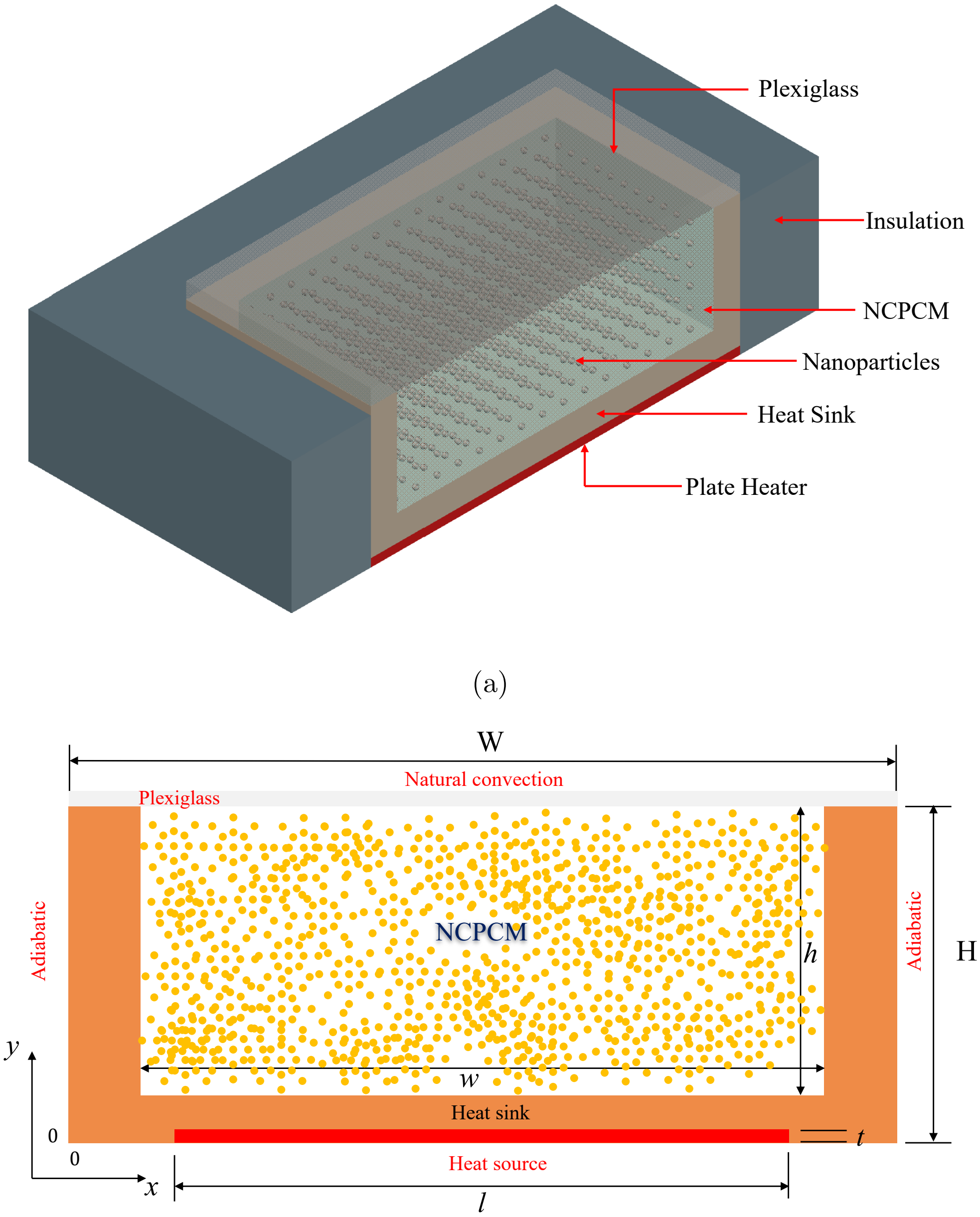

(b)

Figure 1: *(a) A 3D isometric view of NCPCM filled heat sink assembly and (b) physical domain used in current study.*

- The initial temperature of heat sink and NCPCM are the same temperature.
- The thermophysical properties of heat sink, PCM and nanoparticles are constant.
- The NCPCM is considered as colloid suspension which exhibits as a Newtonian fluid. The liquid NCPCM flow regime is $2D$, laminar, unsteady and incompressible.
- The dispersion of nanoparticles in PCM is assumed homogeneous, no agglomeration is considered.

Table 1: Thermophysical properties of PCM and nanoparticles.

Property	**RT–28HC**	**Cu**
T_m(K)	301	–
T_s(K)	302	–
T_l(K)	300	–
L (J/kg)	250,000	–
c_p (J/kg.K)	2000	380
ρ (kg/m^3)	825	8920
k (W/m.K)	0.2	400
μ (Pa.s)	0.0235	–
β (1/K)	0.0006	–

- The nanoparticles and PCM are in local thermal equilibrium and there is no–slip between them.
- The heat sink is considered as solid–state with homogeneous and isotropic properties and thermal conduction heat transfer exists.
- Viscous dissipations are considered negligible.
- Volume change in NCPCM is negligible during phase–change process.
- The Boussinesq approximation is used to model the buoyancy driven force under natural convection as $\rho = \rho_m/\beta(T - T_m) + 1$, where $T_m = (T_s + T_l)/2$.
- No–slip boundary conditions are considered for velocities at the boundaries.
- Adiabatic boundary conditions are assumed from the surroundings.

Based on the above assumptions, the governing equations to model the NCPCM flow motion and temperature variation inside the heat sink are governed by the standard Navier-Stokes and energy equations:

Continuiy:

$$\frac{\partial u}{\partial x} + \frac{\partial v}{\partial y} = 0 \tag{1}$$

Momentum in x–direction:

$$\rho_{ncpcm}\left(\frac{\partial u}{\partial t} + u\frac{\partial u}{\partial x} + v\frac{\partial u}{\partial y}\right) = -\frac{\partial p}{\partial x} + \mu_{ncpcm}\left(\frac{\partial^2 u}{\partial x^2} + \frac{\partial^2 u}{\partial y^2}\right) + S_x \tag{2}$$

Momentum in y–direction:

$$\rho_{ncpcm}\left(\frac{\partial v}{\partial t}+u\frac{\partial v}{\partial x}+v\frac{\partial v}{\partial y}\right)=-\frac{\partial p}{\partial y}+\mu_{ncpcm}\left(\frac{\partial^2 v}{\partial x^2}+\frac{\partial^2 v}{\partial y^2}\right)+(\rho\beta)_{ncpcm}g(T-T_{ref})+S_y \tag{3}$$

where:

$$S_x=A_m\frac{(1-f_l)^2}{f_l^3-0.001}.u \qquad S_y=A_m\frac{(1-f_l)^2}{f_l^3-0.001}.v \tag{4}$$

where, the ρ_{ncpcm}, μ_{ncpcm}, β_{ncpcm} are the density, dynamic viscosity, and thermal expansion coefficient of the NCPCM, respectively; p and g are the pressure and gravitational acceleration, respectively. The S_x and S_y are source terms, defined by Carman–Kozeny relation for flow in porous media, in x and y directions, respectively. The source terms represent a gradual reduction in velocities from a finite value in liquid to zero in solid, over the computational cell that undergoes the phase–change phenomenon. This means that each cell behaves like a porous media whose porosity is equal to liquid–fraction. The A_m is the mush–zone constant which reflecting the morphology of melting front. The value of A_m is chosen of 10^5 present study [23, 29]. Additionally, f_l is the liquid–fraction during the phase–change in temperature interval of $T_s < T < T_l$ and it varies between 0 (solid) to 1 (liquid), which is defined as:

$$f_l=\begin{cases}0 & \text{if} \quad T<T_s\\ \frac{T-T_s}{T_l-T_s} & \text{if} \quad T_s\le T\le T_l\\ 1 & \text{if} \quad T<T_l\end{cases} \tag{5}$$

Energy (liquid–phase):

$$(\rho c_p)_{ncpcm}\left(\frac{\partial T}{\partial t}+u\frac{\partial T}{\partial x}+v\frac{\partial T}{\partial y}\right)=k_{ncpcm}\left(\frac{\partial^2 T}{\partial x^2}+\frac{\partial^2 T}{\partial y^2}\right)-\frac{\partial(\rho\Delta H)_{ncpcm}}{\partial t} \tag{6}$$

Energy (soild–phase):

$$(\rho c_p)_{ncpcm}\left(\frac{\partial T}{\partial t}\right)=k_{ncpcm}\left(\frac{\partial^2 T}{\partial x^2}+\frac{\partial^2 T}{\partial y^2}\right) \tag{7}$$

where, $(\rho c_p)_{ncpcm}$ is the volumetric heat capacity and ΔH_{ncpcm} is the fractional latent–heat of the NCPCM which is expressed in terms of latent–heat of fusion L_{ncpcm} as follows:

$$\Delta H_{ncpcm} = f_l L_{ncpcm} \tag{8}$$

Where

$$\Delta H_{ncpcm} = \begin{cases} 0 & \text{if} \quad T < T_m \\ f_l L_{ncpcm} & \text{if} \quad T \geq T_m \end{cases} \tag{9}$$

Since, the only heat conduction heat transfer mode is considered for heat sink and heat source. Thus, the corresponding governing equations can be written as follow:

Energy (heat sink):

$$(\rho c_p)_{HS} \left(\frac{\partial T}{\partial t} \right) = k_{HS} \left(\frac{\partial^2 T}{\partial x^2} + \frac{\partial^2 T}{\partial y^2} \right) \tag{10}$$

Energy (heat source):

$$(\rho c_p)_{hs} \left(\frac{\partial T}{\partial t} \right) = k_{hs} \left(\frac{\partial^2 T}{\partial x^2} + \frac{\partial^2 T}{\partial y^2} \right) + q^{'''} \tag{11}$$

where, $(\rho c_p)_{HS}$, k_{HS} $(\rho c_p)_{hs}$, and k_{hs} are the volumetric heat capacity and thermal conductivities of heat sink and heat source, respectively.

2.3. Thermophysical properties of NCPCM

The thermophysical properties of NCPCM are changed with the addition of nanoparticles of varying volume fractions. The provided thermophysical properties of pure PCM (RT–28HC) and Cu nanoparticles are listed in Table 1. All the effective properties of NCPCM are constant except thermal conductivity and calculated based on the volume fraction of nanoparticles. The effective density (ρ_{ncpcm}), specific heat capacity ($c_{p_{ncpcm}}$), latent–heat (L_{ncpcm}), and thermal expansion coefficient (β_{ncpcm}) of the NCPCM can be calculated using simple theoretical models of mixtures as follows [18, 19, 20, 30, 31]:

$$\rho_{ncpcm} = \varphi \rho_{np} + (1 - \varphi)\rho_{pcm} \tag{12}$$

$$c_{p_{ncpcm}} = \frac{\varphi(\rho c_p)_{np} + (1 - \varphi)(\rho c_p)_{pcm}}{\rho_{ncpcm}} \tag{13}$$

$$L_{ncpcm} = \frac{(1-\varphi)(\rho L)_{pcm}}{\rho_{ncpcm}} \tag{14}$$

$$\beta_{ncpcm} = \frac{\varphi(\rho\beta)_{np} + (1-\varphi)(\rho\beta)_{pcm}}{\rho_{ncpcm}} \tag{15}$$

$$\mu_{ncpcm} = 0.983 e^{(12.959\varphi)} \mu_{pcm} \tag{16}$$

In above Equations 12–16, φ is the volume fraction of nanoparticles, the subscripts $ncpcm$, np and pcm refer to the NCPCM, nanoparticles, and PCM, respectively. The transient modifications of k_{ncpcm} of NCPCM are evaluated as function of operating temperature, volume fraction and particle size of Cu nanoparticles using a empirical correlations proposed by Vajjha and Das [32], as follows:

$$k_{ncpcm} = \frac{k_{np} + 2k_{pcm} - 2(k_{pcm} - k_{np})\varphi}{k_{np} + 2k_{pcm} + (k_{pcm} - k_{np})\varphi} k_{pcm} + 5 \times 10^4 \beta_k \zeta \varphi \rho_{pcm} c_{p_{pcm}} \sqrt{\frac{BT}{\rho_{np} d_{np}}} f(T, \varphi) \tag{17}$$

where, B is Boltzmann constant which is equal to 1.381×10^{-23} J/K, $\beta_k = 8.4407(100\varphi)^{-1.07304}$, and function $(f(T,\varphi))$ is defined as follows:

$$f(T, \varphi) = (2.8217 \times 10^{-2}\varphi + 3.917 \times 10^{-3})\frac{T}{T_{ref}} + (-3.0669 \times 10^{-2}\varphi - 3.91123 \times 10^{-3}) \tag{18}$$

where, T_{ref} is the reference temperature which is equal to 273.15 K. The first part of Equation 18 relates with Maxwell model to determine the thermal conductivity of solid PCM while second part of Equation 18 accounts the effects of Brownain motion of nanoparticles, nanoparticles size, volume fraction and temperature dependence. Additionally, ζ is a correction factor which comes in Brownian motion term, because there is no Brownian motion in solid–phase. Therefore, the value of ζ is defined as the same as for f_l [33]. The theoretical models have been widely employed to calculate the effective thermophysical properties of nano-PCM or nanocomposite PCM which has been verified in several papers in the literature for nanofluids as well as nano-PCMs. As approved in the experimental study of Vajjha and Das [32], the employed formulation for the effective thermal conductivity fits very well with the valid experimental study with the maximum deviation of 2.8%.

Vajjha and Das [32] experimentally measured the thermal conductivity of nanofluids and developed a model accounts for the effects of nanoparticles size, volume fraction, temperature, nanoparticles and base fluid thermophysical properties and Brownian motion effect of nano-particles which provides a more comprehensive model compared with the earlier models proposed by Maxwell [34], Bruggeman [35], Hamilton and Crosser [36] and Xuan et al. [37] which were significantly a function of nanoparticle volume fraction. Therefore, to have accurate results, the model of Vajjha and Das was employed which were validated with experimental thermal conductivity values. They also compared their experimental results with those of several existing models showing good agreement [38]. This equation is also widely used after its development in different numerical studies in the literature showing the accuracy of this equation [29, 39, 40, 41]. For the viscosity, the experimental model Vajjha et al. [42] was employed which is determined based on the experimental data and also validated with previous models. Vajjha suggested that the model for the viscosity is practical within the range of 20-90 °C and suitable for the proposed model in this study [43]. Other formulations have already been employed in several published numerical studies in the literature in highly reputation journals such as [18, 20, 31, 44]. It should also be noted that in different review papers on Nano-enhanced phase change material, the models of Vajjha et al. for the thermophysical properties of NePCM are approved and verified and thus they were employed in this study.

2.4. Initial and boundary conditions

The initial and boundary conditions applied in current study are labelled in Figure 1. The side walls of the heat sink are defined as an adiabatic boundary condition except the top surface which is undergoes the natural convection effect. Following are the initial and boundary conditions applied in this work to solve the governing equations as follows:

1. Initial conditions

   $t = 0,\ T = T_{ini} = 288.15\ \text{K},\ f_l = 0$

2. Boundary conditions

- No–slip condition at walls: $u = v = 0$

- Adiabatic walls:

  $-k\frac{\partial T}{\partial x}\Big|_{x=0-W} = 0$ Along vertical walls

  $-k\frac{\partial T}{\partial y}\Big|_{\substack{x=0-10,60-70\\ y=0}} = 0$ For bottom

- Natural convection:

$$-k\frac{\partial T}{\partial y}\bigg|_{y=H} = h(T - T_\infty) \qquad \text{Natural convection}$$

- Volumetric heat generation provided from heat source:

$$-k\frac{\partial T}{\partial y}\bigg|_{\substack{x=10-60mm\\ y=0-2mm}} = q'''$$

2.5. Performance evaluation parameters

To estimate the thermal performance of NCPCM based heat sink, four different performance evaluation parameters such as heat storage capacity (Q), heat storage density (q), rate of heat transfer ($\dot{Q}$), and rate of heat transfer density ($\dot{q}$) along with the total melting time (t_{melt}). The total Q is defined as the total thermal energy storage capacity during the pre–sensible heating, latent–heat of fusion, and post–sensible heating of NCPCM. Whereas, q indicates the total thermal energy storage capacity per unit mass of the NCPCM. Since, the pre–sensible heating and latent–heat are the most significant parameters to determine the Q of NCPCM based heat sink whiling charging mode. Therefore, Q and q can be defined by Equations 19 and 20, respectively, as follows [45]:

$$Q = m_{ncpcm}\left(\int_{solid} c_{p_{ncpcm}} dT + f_l L_{ncpcm} + \int_{liquid} c_{p_{ncpcm}} dT\right) \approx m_{ncpcm}[c_{p_{ncpcm}}(T_m - T_i) + f_l L_{ncpcm}] \quad (19)$$

and

$$q = \frac{Q}{m_{ncpcm}} = \frac{m_{ncpcm}\left(\int_{solid} c_{p_{ncpcm}} dT + f_l L_{ncpcm} + \int_{liquid} c_{p_{ncpcm}} dT\right)}{m_{ncpcm}} \approx \frac{m_{ncpcm}[c_{p_{ncpcm}}(T_m - T_i) + f_l L_{ncpcm}]}{m_{ncpcm}} \quad (20)$$

Since, the Q and q can only evaluate the storage capacity of NCPCM based heat sink relative to the mass of NCPCM. However, there is no relationship of total t_{melt} of NCPCM with Q and q. Thus, the overall thermal performance of heat sink cannot be evaluate only with Q and q. Therefore, the effect of t_{melt}, m_{ncpcm}, and Q are combined together to define the rate of heat transfer ($\dot{Q}$) and rate of heat transfer density ($\dot{q}$). The $\dot{Q}$ indicates the total thermal energy storage capacity per unit melting time and $\dot{q}$ is defined as total thermal energy storage capacity per unit melting time and per unit mass of NCPCM, by Equations 21 and 22, respectively, as follows:

$$\dot{Q} = \frac{Q}{t_{melt}} = \frac{m_{ncpcm}\left(\int_{solid} c_{p_{ncpcm}} dT + f_l L_{ncpcm} + \int_{liquid} c_{p_{ncpcm}} dT\right)}{t_{melt}} \approx \frac{m_{ncpcm}[c_{p_{ncpcm}}(T_m - T_i) + f_l L_{ncpcm}]}{t_{melt}} \quad (21)$$

and

$$\dot{q} = \frac{Q}{t_{melt}.m_{ncpcm}} = \frac{m_{ncpcm}\left(\int_{solid} c_{p_{ncpcm}} dT + f_l L_{ncpcm} + \int_{liquid} c_{p_{ncpcm}} dT\right)}{t_{melt}.m_{ncpcm}} \approx \frac{m_{ncpcm}[c_{p_{ncpcm}}(T_m - T_i) + f_l L_{ncpcm}]}{t_{melt}.m_{ncpcm}} \quad (22)$$

2.6. Numerical procedure and model validation

In current study, the developed governing equations were solved using a commercial computational fluid dynamics (CFD) package ANSYS–FLUENT 19.1. The enthalpy–porosity method was adopted to model the effect of phase–change process in NCPCM based heat sink. In this method, a fixed grid is considered while solution of the governing equations which are varied for both solid and liquids phases. Finite volume method (FVM) scheme was considered to discretize the conservation equations of continuity, momentum and energy with double precision. The mushy zone is modelled as a "pseudo" porous medium which exhibits the porosity equal to the liquid–fraction. The porosity increases from 0 to 1 respecting the solid to liquid phases, respectively; as the PCM melts and velocities develops from zero. The PRESSURE–BASED method is select to discretize the governing equations from Eq. 1–11 which is recommended for incompressible flow with high–order Quadratic Upstream Interpolation for Convective Kinematics (QUICK) differencing scheme presented by Leonard [46]. The Semi-Implicit Pressure-Linked Equation (SIMPLE) algorithm was adopted for pressure–velocity coupling by Patanker [47]. The PRESTO (PREssure STaggering Option) scheme was adopted for pressure correction equation. The User–defined function (UFD) was written in C++ language to account the effective thermal conductivity of NCPCM because of the dispersion of Cu nanoparticles. The gravity effects were also considered and second–order upwind difference scheme was adopted to discretize convective terms in momentum and energy equations. A optimum mesh size and time–step of 54087 elements and 0.1s were considered and in the current study [23]. The under–relaxation factors were set as 0.3, 0.6, 0.9 and 1.0 for pressure, velocity, liquid–fraction and thermal energy, respectively. The convergence criteria are set to 10^{-4}, 10^{-4} and 10^{-6} for continuity, momentum and energy equations, respectively.

The numerical model adopted in current study is validated with experimental results using an unfinned heat sink filled with PCM at $\varphi = 0.00$. The similar initial conditions, boundary conditions and thermophysical properties of materials are adopted in this work to validate the results. The RT–35HC is selected as a PCM with melting temperature of 35 °C and a input power level of 5 W is applied at the base of heat sink. The results of average heat sink temperature are compared of both and numerical studies as shown in Figure 2. It can be seen that an acceptable agreement is achieved between the experimental results and the present study. A few discrepancies are observed before the melting and later in phase–change phase which are due to achieving perfectly adiabatic boundary conditions while experimentation and presence impurities in RT–35HC compared with the ideal thermophysical properties provided in numerical study.

To validate the code related to the use of nanoparticles, the results of Mahdi and Nsofore [30] are used for comparison. They simulated the melting process inside a horizontal triple-tube LHS unit using RT82 and 2% Al_2O_3 nanoparticles where the temperatures of the inner and outer tubes are considered 90 °C. As shown in Figure 4, the present results are in excellent agreement with Ref. [30].

3. Results and discussion

3.1. Evaluation of isotherms

The instantaneous variations of average heat sink temperature (T_{HS}) is shown in Figure 4 for different volume fractions (φ = 0.00, 0.01, 0.03, and 0.05) of Cu nanoparticles. The isotherms of NCPCM heat sink are grouped at every 600 s of melting process for each φ as follows:

- At $t = 1500$s, the variation in T_{HS} can been see from lower to higher temperature over the surface of the heat sink which is due to the conduction and convection heat transfer modes. The conduction heat transfer process can be seen clearly at the boundaries of PCM and heat sink interaction because of the higher temperature gradient. A

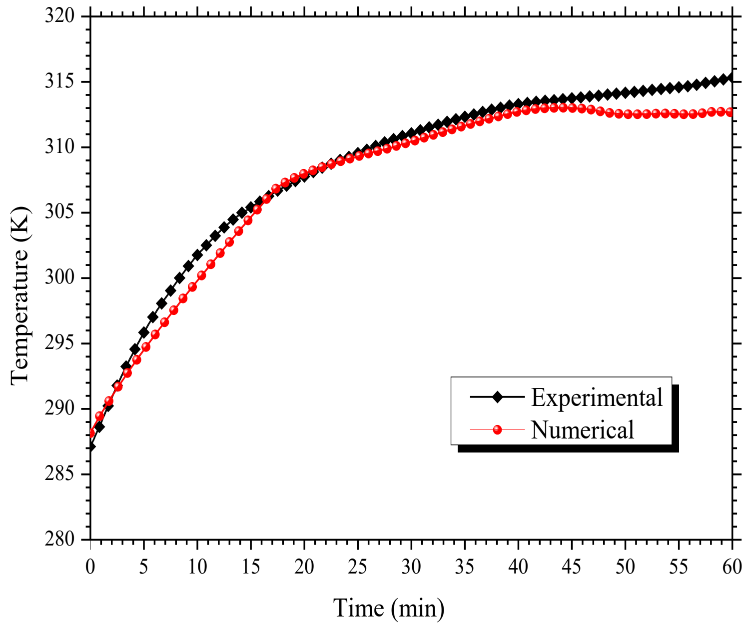

Figure 2: *Validation of present study with experimental results of an unfinned heat sink filled with PCM at* $\varphi = 0.00$.

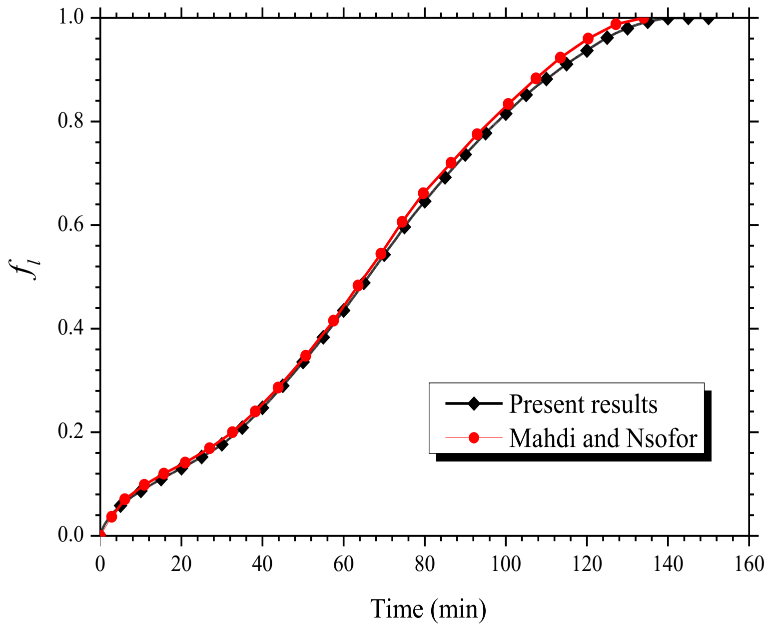

Figure 3: *Validation of present results of NCPCM simulation compared with Mahdi and Nsofor at* $\varphi = 0.02$ *[30].*

uniform isotherms distribution can be seen between the solid and liquid PCM zones specially at $\varphi = 0.05$. However, the dominant heat transfer process is because of pure conduction. Since, the addition of different nanoparticles φ do not show the a noticeable distribution of isotherms inside the heat sink which indicates that presence of nanoparticles are just to enhance the heat transfer rate by conduction.

- At $t = 2100$s, the both conduction and convection heat transfer modes can be seen in isotherms and PCM tend to depart the uniformity in shape which is the initiating of natural convection heat transfer of NCPCM inside the heat sink. At the bottom of heat sink, the circular pattern of isotherms can be observed which is due to the buoyancy force which are developed by the temperature gradient across the heat sink base and gravity force.

- At $t = 2700$s, the more dominant convection patterns of isotherms can be seen while heat transfer process of NCPCM heat sink. The more deformed and circular patterns are increased in size because of the growing role of convection heat transfer in melt zone. The relatively cold PCM at the upper part of heat sink moves downward under the gravity effect while melting which is replaced by a melted PCM moving upward under the effect of buoyancy force. At this stage the PCM temperature is affected by both conduction and natural convection heat transfer modes, however, heat conduction mode is dominant until the isotherms do not keep a unified colour.

- At $t = 3300$s, the more uniform isotherms are observed in shape and colour become of increasing effect natural convection inside the PCM melt zone. It can be observed that increasing the φ while PCM melting process, the isotherms show there is no significant influence of circulating patterns. This is because of increase of the effective thermal conductivity of NCPCM by adding the nanoparticles which enhance the conduction phenomenon and PCM melting. However, by the adding the nanoparticles, the viscosity of the PCM is increased which tend to reduce the movement of liquid PCM inside the heat sink resulting in weakens the natural convection heat transfer contribution. A closer look reveals that upper part of the heat sink has the higher temperature zone as compared to the central zone which show that PCM melt is dominant because of exceeding effect to buoyancy force rather than gravity force. In general, it can be seen that nanoparticles improves the thermal conduction heat transfer with the less effect of natural convection inside the heat sink.

3.2. Evaluation of liquid–fraction

The solid–liquid interface of NCPCM heat sink is illustrated though f_l contours presented in 5. The melting phenomenon of PCM at different φ of 0.00, 0.01, 0.03, and 0.05 of Cu nanoparticles is presented at different time stages to better understand influence of nanoparticles in PCM as follows:

- At t = 1500s, the solid liquid zones of PCM can be seen clearly representing in blue and red colours, respectively. The PCM melting layers at the bottom and sides walls can be observed and circulating patterns of liquid PCM are found at the bottom of the heat sink due the effect of buoyancy and gravity forces. Since the heat transfer occurs from bottom and sides of heat sink which is mainly due to conduction heat transfer between solids walls and solid PCM layers.

- At t =2100s, the increasing tend of circulating patterns of liquid PCM are observed which is because of the increasing effect of buoyancy force developed as a result of temperature gradient. Since, the addition of nanoparticles enhance the thermal conductivity of NCPCM as the well as the viscosity of NCPCM which enhance the heat transfer rate and also affects the melt movement of PCM. Therefore, conduction heat transfer mode dominates over convection mode.

- At t = 2700s, the significance of natural convection is noticeable by appearing the more deformation and size of rotating circles of melted PCM during melting process of NCPCM. In addition, a regular melting patterns of solid–liquid PCM can be seen with the increase of nanoparticles volume fraction. A closer look reveals that relative cold PCM moves downward from solid–liquid interface because of gravitational effect which improves the complete melting of PCM. This movement of melted PCM enhances the rate of PCM melting at the bottom half of the heat sink compared to the upper half.

- At t = 3300s, the higher rate of f_l of NCPCM is obtained in most of the part of heat sink domain which shows the dominant contribution of natural convection heat transfer because of the influence of buoyancy effects. There is still movement of cold or relative less melted PCM towards the bottom because of gravity effects, however, there is a absence of circulating patterns of melted PCM and uniform melting is observed specially at $\varphi = 0.05$. It can be observed that the increasing the φ of nanoparticles increases the size of melted NCPCM and more symmetrical melting patten is observed because of viscous effects.

- At t = 3600s, the complete melting of NCPCM is obtained for 0.01, 0.03, and 0.05 φ because of conduction and natural convection contribution. Since, the addition of nanoparticles improves the thermal conductivity of PCM, thus, it improves the conductive heat transfer rate within the PCM and faster melting is achieved. Contrarily,

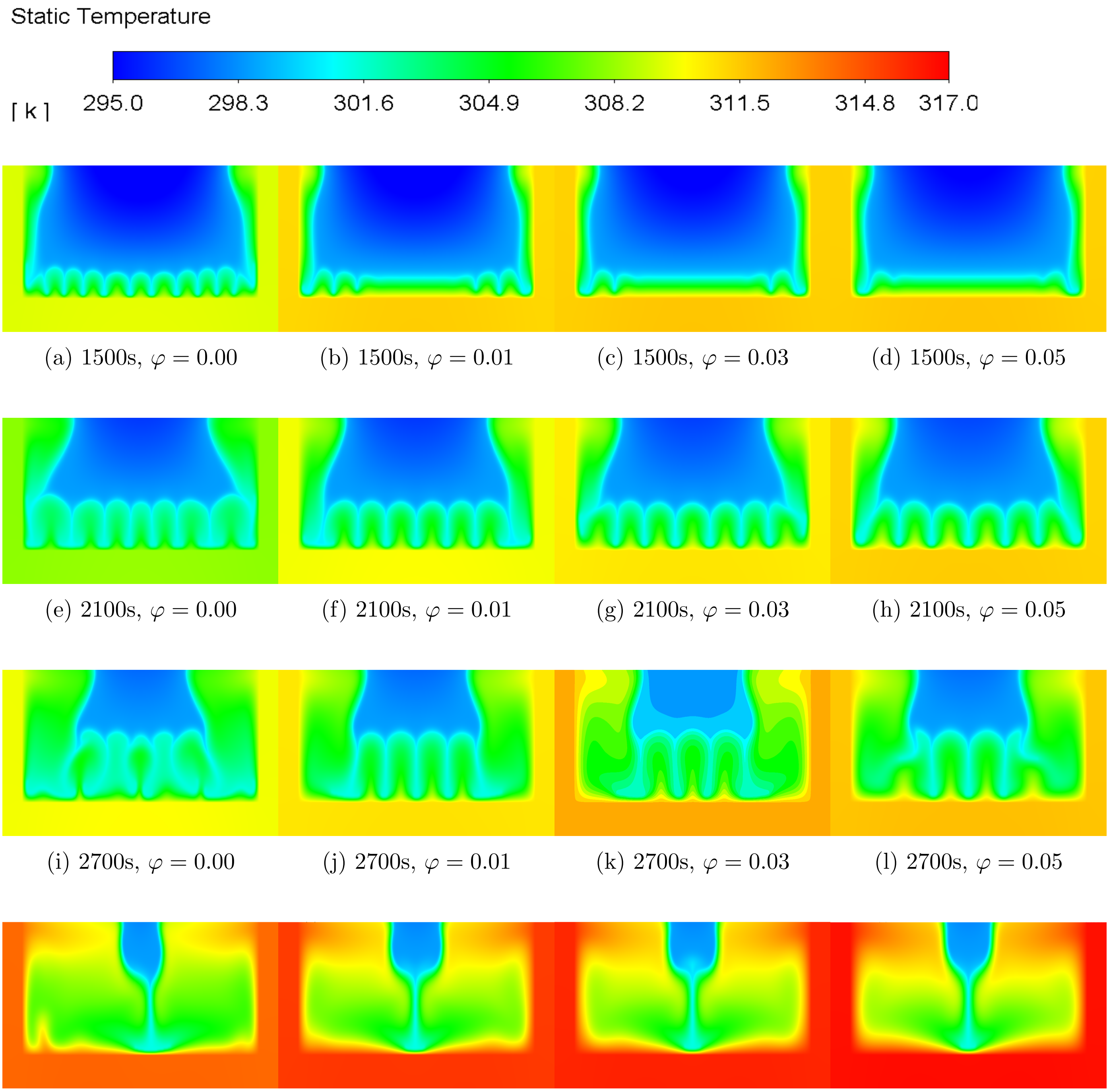

(a) 1500s, $\varphi = 0.00$ (b) 1500s, $\varphi = 0.01$ (c) 1500s, $\varphi = 0.03$ (d) 1500s, $\varphi = 0.05$

(e) 2100s, $\varphi = 0.00$ (f) 2100s, $\varphi = 0.01$ (g) 2100s, $\varphi = 0.03$ (h) 2100s, $\varphi = 0.05$

(i) 2700s, $\varphi = 0.00$ (j) 2700s, $\varphi = 0.01$ (k) 2700s, $\varphi = 0.03$ (l) 2700s, $\varphi = 0.05$

(m) 3300s, $\varphi = 0.00$ (n) 3300s, $\varphi = 0.01$ (o) 3300s, $\varphi = 0.03$ (p) 3300s, $\varphi = 0.05$

Figure 4: *Variation of isotherms contours at various t and φ of NCPCM based heat sink.*

at $\varphi = 0.00$, there is a still little portion of unmelted PCM which results in to decrease the heat sink temperature suddenly. In short, the effect of nanoparticles appear more significantly as the φ of nanoparticles increases and time progresses while the melting process of NCPCM based heat sink.

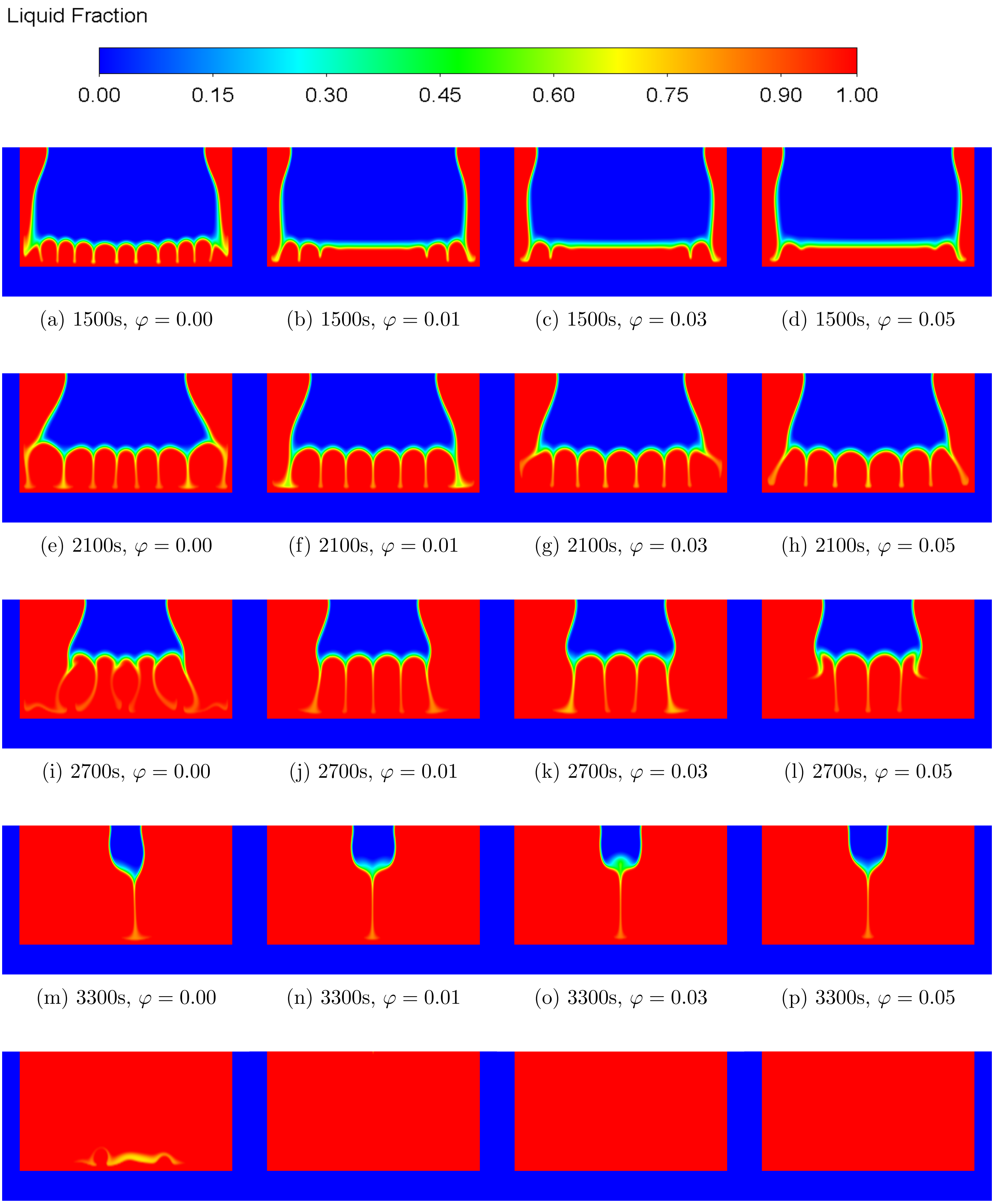

(a) 1500s, $\varphi = 0.00$ (b) 1500s, $\varphi = 0.01$ (c) 1500s, $\varphi = 0.03$ (d) 1500s, $\varphi = 0.05$

(e) 2100s, $\varphi = 0.00$ (f) 2100s, $\varphi = 0.01$ (g) 2100s, $\varphi = 0.03$ (h) 2100s, $\varphi = 0.05$

(i) 2700s, $\varphi = 0.00$ (j) 2700s, $\varphi = 0.01$ (k) 2700s, $\varphi = 0.03$ (l) 2700s, $\varphi = 0.05$

(m) 3300s, $\varphi = 0.00$ (n) 3300s, $\varphi = 0.01$ (o) 3300s, $\varphi = 0.03$ (p) 3300s, $\varphi = 0.05$

(q) 3600s, $\varphi = 0.00$ (r) 3600s, $\varphi = 0.01$ (s) 3600s, $\varphi = 0.03$ (t) 3600s, $\varphi = 0.05$

Figure 5: *Variation of f_l at various t and φ of NCPCM based heat sink.*

3.3. Evaluation of average T_{HS} and T_{ncpcm} of NCPCM based heat sink.

The distribution of average T_{HS} and T_{ncpcm} for different φ of nanoparticles are presented in Figure 6a and 6b, respectively, at a constant input power level. A higher temperature rise is observed with the increase of φ at the end of melting after 3600 s for both T_{HS} and T_{ncpcm}. Additionally, it can be seen that the lower T_{HS} and T_{ncpcm} are observed as φ increases from 0.01 to 0.05, however, these are higher than at $\varphi = 0.00$. The T_{HS} of 334.5, 339.77, 340.54, and 341.23 K at φ of 0.00, 0.01, 0.03, and 0.05, respectively. Similarly, the T_{ncpcm} of 329.51, 334.61, 335.14, and 335.69 K at φ of 0.00, 0.01, 0.03, and 0.05, respectively. The higher temperature rise at φ of 0.01, 0.03, and 0.05 is because of the increase of effective ρ_{ncpcm}, $\rho_{ncpcm} c_{ncpcm}$ and decrease of L_{ncpcm}. Moreover, the k_{ncpcm} increases with the increase of time and temperature as φ increases from 0.01 to 0.05. This result in increase of the T_{HS} and T_{ncpcm} and decrease of L_{ncpcm} with the increase of time. Figure 6 also illustrates that a uniform melting is observed during phase–change process with the increase of φ. The results suggest that a heat sink with NCPCM filling is more effective than the pure PCM which can be more efficient for passive cooling electronic components.

3.4. Evaluation of f_l and t_{melt} of NCPCM based heat sink

The results of f_l and t_{melt} are presented in 7a and 7b, respectively, at constant power level. It can be seen that the higher f_l is observed with the increase of φ which results in reduce the t_{melt} of NCPCM. The complete t_{melt} of NCPCM is obtained of 3625, 3590, 3575, 3555 s for φ of 0.00, 0.01, 0.03, and 0.05, respectively, a shown in Figure 7a. The comparison t_{melt} of NCPCM at φ of 0.00, 0.01, 0.03, and 0.05 is shown in Figure 7b. The t_{melt} of 3320, 3275, 3260, 3235 s is obtained for φ of 0.00, 0.01, 0.03, and 0.05, respectively. This illustrates that with the increase of φ, the t_{melt} reduces, as expected. The reduction in t_{melt} of NCPCM based heat sink is obtained of -1.36%, -1.81%, and -2.56% at $\varphi = 0.01$, 0.03, and 0.05, respectively, compared with pure PCM based heat sink.

3.5. Evaluation of Q and q of NCPCM based heat sink

The comparison of Q and q of NCPCM based heat sink at different φ is shown in Figure 8. The heat storage analysis presents the amount of heat absorbed by the NCPCM heat sink generated by a electronic component during operation. It can be seen that heat storage capacity increases at $\varphi = 0.01$ and 0.03, however, a slight decrease is obtained at 0.05 of Cu nanoparticles. This variation in results is because of the change in total mass of the PCM by adding the nanoparticles. The Q is composed of the total heat stored energy during

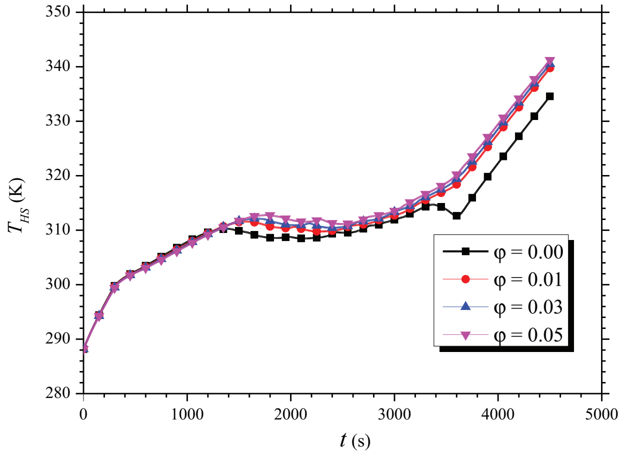

(a)

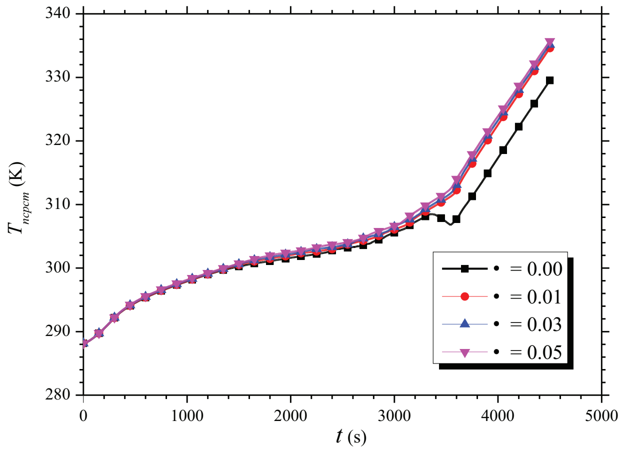

(b)

Figure 6: *Variation of average (a) T_{HS} and (b) T_{ncpcm} of NCPCM based heat sink.*

sensible heating and latent–heating of the NCPCM, as mentioned in Equation 19. The total Q is calculated of 287.28, 292.66, 289.53, and 286.33 kJ of corresponding φ of 0.00, 0.01, 0.03, and 0.05. The variations for 0.01, 0.03, and 0.05 φ of Cu nanoparticles are obtained of 1.87%, 0.78%, and −0.33%, respectively, compared with 0.00 or pure PCM based heat sink. Since, the variations in Q is very small, however, the increasing effect of NCPCM mass cannot be ignored due the increase of the effective ρ_{ncpcm} with the addition of Cu nanoparticles. Compared with pure PCM, the mass of PCM increases by 9.81%, 29.44%, and 49.06% by adding the φ of 0.01, 0.03, and 0.05, respectively. Therefore, the results q, defined by Equation 20, are shown in Figure 8 for different φ. The q reduces significantly with the addition of Cu nanoparticles and depends on the amount of φ. The q is reduced 290.19, 269.20, 225.95, and 194.03 kJ/kg of corresponding φ of 0.00, 0.01, 0.03, and 0.05. For 0.01, 0.03, and 0.05 φ of Cu nanoparticles, the q is dropped of −7.23%, −22.14%, and −33.14%, respectively, compared with 0.00 or pure PCM based heat sink. The results are

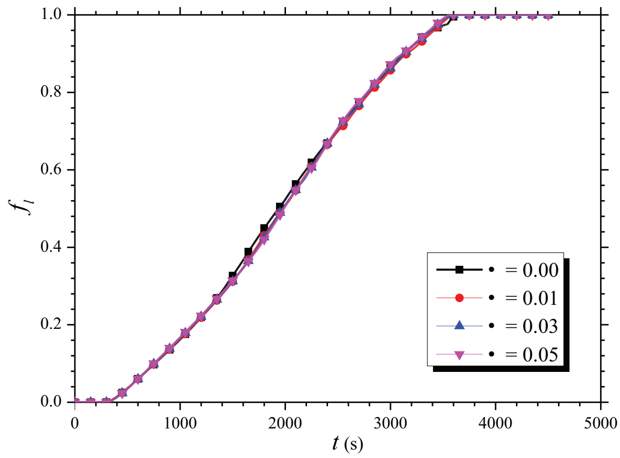

(a)

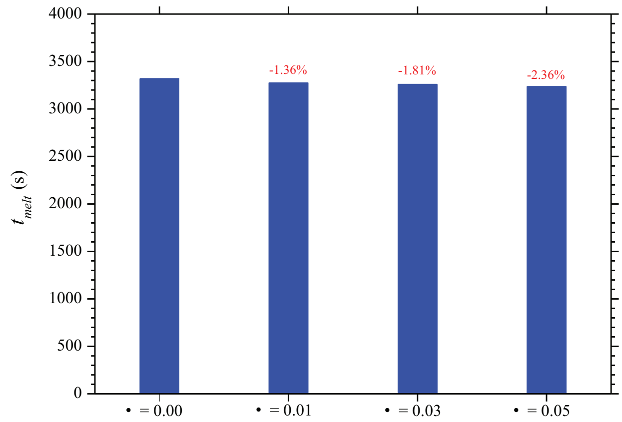

(b)

Figure 7: *Variation of (a) f_l and (b) t_{melt} of NCPCM based heat sink.*

attributed to the product of effective ρ_{ncpcm} and c_{ncpcm}, $\rho_{ncpcm}c_{ncpcm}$. The results of Q and q indicate that even though the addition of nanoparticles increases the mass of PCM and reduces the effective c_{ncpcm} of NCPCM, however, the effect of ρ_{ncpcm} is more than the c_{ncpcm}. Therefore, it is suggested to use the $\varphi = 0.01$ of Cu nanoparticles for NCPCM heat sink for passive cooling application of electronic component.

3.6. Evaluation of $\dot{Q}$ and $\dot{q}$ of NCPCM based heat sink.

The comparison of $\dot{Q}$ and $\dot{q}$ is presented in Figure 9. The $\dot{Q}$ and $\dot{q}$ are calculated using Equations 21 and 22, respectively, to evaluate the rate of cooling performance or enhancement in heat transfer of a NCPCM based heat sink. It can be seen that rate of heat transfer increases with the addition of Cu nanoparticles. However, it decreases slightly from 0.01 to 0.05 due to the decrease of effective c_{ncpcm} of NCPCM. The $\dot{Q}$ is obtained of 79.25, 81.52, 80.99, and 80.54 W for φ of 0.00, 0.01, 0.03, and 0.05, respectively. The enhancement in $\dot{Q}$ is obtained of 2.86%, 2.19%, and 1.63% for 0.01, 0.03, and 0.05, respectively, of φ of Cu

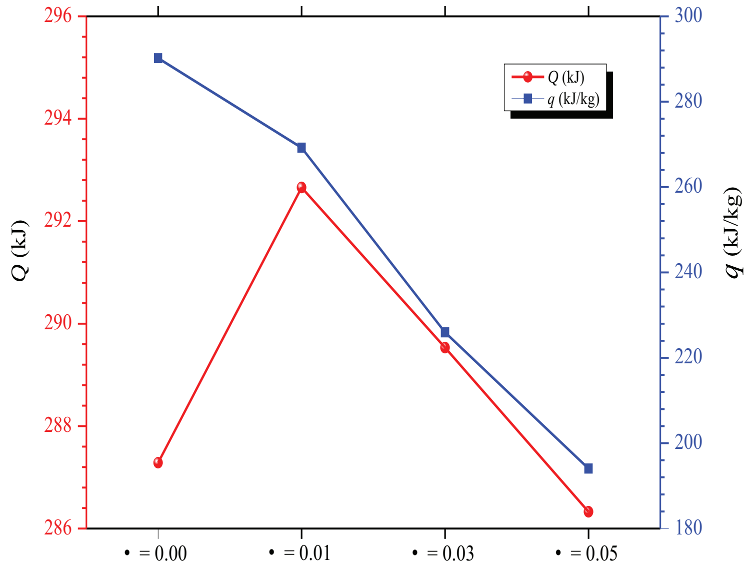

Figure 8: *Comparison of Q and q of a NCPCM based heat sink.*

nanoparticles. In addition, the effect of $\dot{q}$ with different PCM masses, defined by Equation 22, is proposed and assessed for different φ. Since, PCM mass increases with the increase of φ, therefore, the $\dot{q}$ decreases. The amount of $\dot{q}$ is obtained of 80.05, 74.99, 63.20, and 54.58 W for φ of 0.00, 0.01, 0.03, and 0.05, respectively. With the addition of 0.01, 0.03, and 0.05 Cu nanoparticles, the $\dot{q}$ is dropped of -6.33%, -21.05%, and -31.82%, respectively, as expected, as shown in Figure 9. The results indicate that, at $\varphi = 0.01$ of Cu nanoparticles, higher and lower trend is obtained between $\dot{Q}$ and $\dot{q}$, respectively, which is preferable for passive cooling electronic device in practical applications.

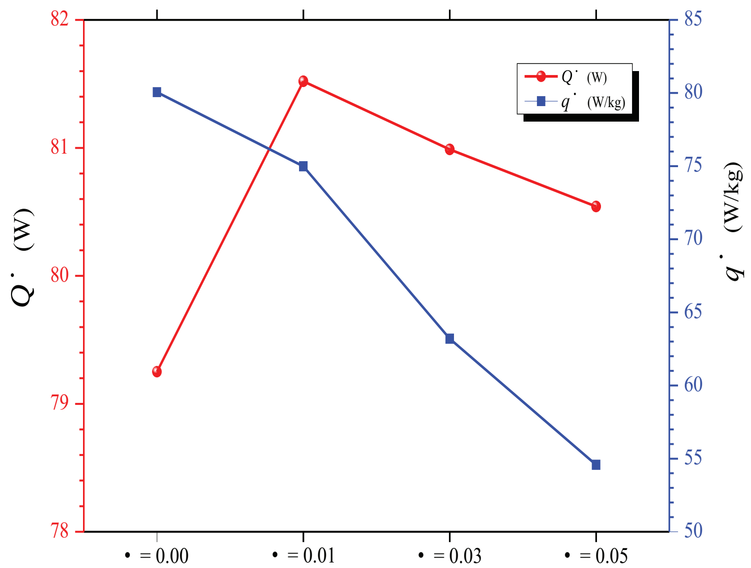

Figure 9: *Comparison of $\dot{Q}$ and $\dot{q}$ of a NCPCM based heat sink.*

4. Conclusions

A transient $2D$ numerical study is conducted to investigate the influence of nanoparticles in PCM based heat sink to evaluate the thermal cooling performance of electronic components. Different volume fractions of 0.00, 0.01, 0.03, and 0.05 of Cu nanoparticles are varied with at a constant power level of 5 W. The contours of isotherms and transient liquid–fraction are presented for different time intervals and volume fractions of nanoparticles. Different thermal performance evaluation indicators such melting time, heat storage capacity, heat storage density, rate of heat transfer, and rate of heat transfer density were evaluated. Following are the key findings drawn from the results:

- The addition of nanoparticles enhanced the melting rate and thermal conduction mode of PCM with the increase of volume fraction because of the enhancement in effective thermal conductivity and viscous effects of NCPCM. Addition of nanoparticles improved the uniformity in melting process.

- A temperature rise was observed with the increase of φ at the end of melting process for both heat sink and NCPCM cases. The lower heat sink and NCPCM temperatures were achieved with the increase of volume fraction of nanoparticles.

- The melting time was reduced with the increase of nanoparticles volume fraction and the reduction in melting time was obtained of -1.36%, -1.81%, and -2.56% at 0.01, 0.03, and 0.05, respectively, compared with pure PCM based heat sink.

- The higher heat storage capacity was obtained with 0.01 volume fraction and enhancement of 1.87% was achieved compared with pure PCM. The heat storage capacity density was decreased with addition of nanoparticles and minimum reduction of -7.23% was obtained with 0.01 volume fraction.

- The enhancement in rate of heat transfer was obtained of 2.86%, 2.19% and 1.63%; and reduction in rate of heat transfer density was obtained of -6.33%, -21.05% and -31.82% with 0.01, 0.03, and 0.05 volume fraction of Cu nanoparticles, respectively. The results suggest that Cu nanoparticles of 0.01, the rate of heat transfer is higher and rate heat transfer density is lower which is preferable for passive cooling electronic device in practical application.

To sum up, it is revealed that the addition of Cu nanoparticles in PCM improve the heat flow and solid-liquid melting transformation with more uniformly. The lower heat sink base temperature can be achieved with NCPCM based heat sink, however, this variation is not so significant with only the addition of nanoparticles. Thus, it is suggested to combine metallic fins and/or metal-foams along with the nanoparticles. Moreover, the better enhancement in conjugate heat transfer rate is obtained with NCPCM based heat sink compared with pure PCM based heat sink. Thus, this paper provide guidelines toward the usage of PCM-based electronic cooling applications by providing an in-depth system level performance analysis.

Acknowledgement

This research is facilitated by the University of Nottingham, UK research infrastructure. The first author (Adeel Arshad) acknowledges the University of Nottingham for awarding him the *Faculty of Engineering Research Excellence PhD Scholarship* to pursue a Ph.D. research program.

Conflict of interest

The authors declare no conflict of interest regarding this research article.

References

[1] S. S. Murshed, C. N. de Castro, A critical review of traditional and emerging techniques and fluids for electronics cooling, Renewable and Sustainable Energy Reviews 78 (2017) 821–833. doi:10.1016/j.rser.2017.04.112.

[2] M. Pedram, S. Nazarian, Thermal modeling, analysis, and management in VLSI circuits: Principles and methods, Proceedings of the IEEE 94 (8) (2006) 1487–1501. doi:10.1109/jproc.2006.879797.

[3] P. K. S. Rathore, S. K. Shukla, Enhanced thermophysical properties of organic PCM through shape stabilization for thermal energy storage in buildings: A state of the art review, Energy and Buildings 236 (2021) 110799. doi:10.1016/j.enbuild.2021.110799.

[4] S. Adibpour, A. Raisi, B. Ghasemi, A. Sajadi, G. Rosengarten, Experimental investigation of the performance of a sun tracking photovoltaic panel with phase change material, Renewable Energy 165 (2021) 321–333. doi:10.1016/j.renene.2020.11.022.

[5] P. Royo, L. Acevedo, Á. J. Arnal, M. Diaz-Ramírez, T. García-Armingol, V. J. Ferreira, G. Ferreira, A. M. López-Sabirón, Decision support system of innovative high-temperature latent heat storage for waste heat recovery in the energy-intensive industry, Energies 14 (2) (2021) 365. doi:10.3390/en14020365.

[6] F. Bentivoglio, S. Rouge, O. Soriano, A. T. de Sousa, Design and operation of a 180 kWh PCM heat storage at the flaubert substation of the grenoble urban heating network, Applied Thermal Engineering 185 (2021) 116402. doi:10.1016/j.applthermaleng.2020.116402.

[7] E. Guelpa, Impact of thermal masses on the peak load in district heating systems, Energy 214 (2021) 118849. doi:10.1016/j.energy.2020.118849.

[8] D. Qin, Z. Liu, Y. Zhou, Z. Yan, D. Chen, G. Zhang, Dynamic performance of a novel air-soil heat exchanger coupling with diversified energy storage components—modelling development, experimental verification, parametrical design and robust operation, Renewable Energy 167 (2021) 542–557. doi:10.1016/j.renene.2020.11.113.

[9] H. M. Ali, A. Arshad, M. M. Janjua, W. Baig, U. Sajjad, Thermal performance of LHSU for electronics under steady and transient operations modes, International Journal of Heat and Mass Transfer 127 (2018) 1223–1232. doi:10.1016/j.ijheatmasstransfer.2018.06.120.

[10] R. Kalbasi, Introducing a novel heat sink comprising PCM and air - adapted to electronic device thermal management, International Journal of Heat and Mass Transfer 169 (2021) 120914. doi:10.1016/j.ijheatmasstransfer.2021.120914.

[11] A. Arshad, M. Jabbal, Y. Yan, Preparation and characteristics evaluation of mono and hybrid nano-enhanced phase change materials (NePCMs) for thermal management of microelectronics, Energy Conversion and Management 205 (2020) 112444. doi:10.1016/j.enconman.2019.112444.

[12] A. Arshad, M. Jabbal, Y. Yan, Thermophysical characteristics and application of metallic-oxide based mono and hybrid nanocomposite phase change materials for thermal management systems, Applied Thermal Engineering 181 (2020) 115999. doi:10.1016/j.applthermaleng.2020.115999.

[13] M. Kibria, M. Anisur, M. Mahfuz, R. Saidur, I. Metselaar, A review on thermophysical properties of nanoparticle dispersed phase change materials, Energy Conversion and Management 95 (2015) 69–89. doi:10.1016/j.enconman.2015.02.028.

[14] A. Arshad, M. Jabbal, L. Shi, J. Darkwa, N. J. Weston, Y. Yan, Development of tio2/rt–35hc based nanocomposite phase change materials (ncpcms) for thermal management applications, Sustainable Energy Technologies and Assessments (2020) 100865doi:10.1016/j.seta.2020.100865.

[15] S. C. Lin, H. H. Al-Kayiem, Thermophysical properties of nanoparticles-phase change material compositions for thermal energy storage, Applied Mechanics and Materials 232 (2012) 127–131. doi:10.4028/www.scientific.net/amm.232.127.

[16] S. C. Lin, H. H. Al-Kayiem, Evaluation of copper nanoparticles – paraffin wax compositions for solar thermal energy storage, Solar Energy 132 (2016) 267–278. doi:10.1016/j.solener.2016.03.004.

[17] L. Colla, D. Ercole, L. Fedele, S. Mancin, O. Manca, S. Bobbo, Nano-phase change

materials for electronics cooling applications, Journal of Heat Transfer 139 (5). doi:10.1115/1.4036017.

[18] N. S. Bondareva, B. Buonomo, O. Manca, M. A. Sheremet, Heat transfer inside cooling system based on phase change material with alumina nanoparticles, Applied Thermal Engineering 144 (2018) 972–981. doi:10.1016/j.applthermaleng.2018.09.002.

[19] N. S. Bondareva, B. Buonomo, O. Manca, M. A. Sheremet, Heat transfer performance of the finned nano-enhanced phase change material system under the inclination influence, International Journal of Heat and Mass Transfer 135 (2019) 1063–1072. doi:10.1016/j.ijheatmasstransfer.2019.02.045.

[20] J. M. Mahdi, E. C. Nsofor, Solidification of a PCM with nanoparticles in triplex-tube thermal energy storage system, Applied Thermal Engineering 108 (2016) 596–604. doi:10.1016/j.applthermaleng.2016.07.130.

[21] A. Ebrahimi, A. Dadvand, Simulation of melting of a nano-enhanced phase change material (NePCM) in a square cavity with two heat source–sink pairs, Alexandria Engineering Journal 54 (4) (2015) 1003–1017. doi:10.1016/j.aej.2015.09.007.

[22] S. Hosseinizadeh, A. R. Darzi, F. Tan, Numerical investigations of unconstrained melting of nano-enhanced phase change material (NEPCM) inside a spherical container, International Journal of Thermal Sciences 51 (2012) 77–83. doi:10.1016/j.ijthermalsci.2011.08.006.

[23] A. Arshad, M. Jabbal, P. T. Sardari, M. A. Bashir, H. Faraji, Y. Yan, Transient simulation of finned heat sinks embedded with PCM for electronics cooling, Thermal Science and Engineering Progress 18 (2020) 100520. doi:10.1016/j.tsep.2020.100520.

[24] A. Arshad, H. M. Ali, W.-M. Yan, A. K. Hussein, M. Ahmadlouydarab, An experimental study of enhanced heat sinks for thermal management using n-eicosane as phase change material, Applied Thermal Engineering 132 (2018) 52–66. doi:10.1016/j.applthermaleng.2017.12.066.

[25] A. Arshad, H. M. Ali, S. Khushnood, M. Jabbal, Experimental investigation of PCM based round pin-fin heat sinks for thermal management of electronics: Effect of pin-fin diameter, International Journal of Heat and Mass Transfer 117 (2018) 861–872. doi:10.1016/j.ijheatmasstransfer.2017.10.008.

[26] A. Arshad, H. M. Ali, M. Ali, S. Manzoor, Thermal performance of phase change material (PCM) based pin-finned heat sinks for electronics devices: Effect of pin thickness and PCM volume fraction, Applied Thermal Engineering 112 (2017) 143–155. doi:10.1016/j.applthermaleng.2016.10.090.

[27] H. Faraji, M. Faraji, M. E. Alami, Numerical survey of the melting driven natural convection using generation heat source: Application to the passive cooling of electronics using nano-enhanced phase change material, Journal of Thermal Science and Engineering Applications 12 (2). doi:10.1115/1.4044167.

[28] H. Faraji, M. Faraji, M. E. Alami, Y. Hariti, A. Arshad, A. Hader, A. Benkaddour, Cooling of recent microprocessors by the fusion of nano-enhanced phase change materials, Materials Today: Proceedingsdoi:10.1016/j.matpr.2020.04.342.

[29] J. M. Mahdi, H. I. Mohammed, E. T. Hashim, P. Talebizadehsardari, E. C. Nsofor, Solidification enhancement with multiple PCMs, cascaded metal foam and nanoparticles in the shell-and-tube energy storage system, Applied Energy 257 (2020) 113993. doi:10.1016/j.apenergy.2019.113993.

[30] J. M. Mahdi, E. C. Nsofor, Melting enhancement in triplex-tube latent thermal energy storage system using nanoparticles-fins combination, International Journal of Heat and Mass Transfer 109 (2017) 417–427. doi:10.1016/j.ijheatmasstransfer.2017.02.016.

[31] M. Arıcı, E. Ttnc, Ç. Yıldız, D. Li, Enhancement of PCM melting rate via internal fin and nanoparticles, International Journal of Heat and Mass Transfer 156 (2020) 119845. doi:10.1016/j.ijheatmasstransfer.2020.119845.

[32] R. S. Vajjha, D. K. Das, Experimental determination of thermal conductivity of three nanofluids and development of new correlations, International Journal of Heat and Mass Transfer 52 (21-22) (2009) 4675–4682. doi:10.1016/j.ijheatmasstransfer.2009.06.027.

[33] A. V. Arasu, A. S. Mujumdar, Numerical study on melting of paraffin wax with al2o3 in a square enclosure, International Communications in Heat and Mass Transfer 39 (1) (2012) 8–16. doi:10.1016/j.icheatmasstransfer.2011.09.013.

[34] M. Levin, M. Miller, Maxwell a treatise on electricity and magnetism, Uspekhi Fizicheskikh Nauk 135 (3) (1981) 425–440.

[35] D. A. G. Bruggeman, Berechnung verschiedener physikalischer konstanten von heterogenen substanzen. i. dielektrizittskonstanten und leitfhigkeiten der mischkrper aus isotropen substanzen, Annalen der Physik 416 (7) (1935) 636–664. doi:10.1002/andp.19354160705.

[36] R. L. Hamilton, O. K. Crosser, Thermal conductivity of heterogeneous two-component systems, Industrial & Engineering Chemistry Fundamentals 1 (3) (1962) 187–191. doi:10.1021/i160003a005.

[37] Y. Xuan, Q. Li, W. Hu, Aggregation structure and thermal conductivity of nanofluids, AIChE Journal 49 (4) (2003) 1038–1043. doi:10.1002/aic.690490420.

[38] M. Al-Maghalseh, K. Mahkamov, Methods of heat transfer intensification in PCM thermal storage systems: Review paper, Renewable and Sustainable Energy Reviews 92 (2018) 62–94. doi:10.1016/j.rser.2018.04.064.

[39] J. M. Mahdi, S. Lohrasbi, D. D. Ganji, E. C. Nsofor, Accelerated melting of PCM in energy storage systems via novel configuration of fins in the triplex-tube heat exchanger, International Journal of Heat and Mass Transfer 124 (2018) 663–676. doi:10.1016/j.ijheatmasstransfer.2018.03.095.

[40] Z. Khan, Z. A. Khan, P. Sewell, Heat transfer evaluation of metal oxides based nano-PCMs for latent heat storage system application, International Journal of Heat and Mass Transfer 144 (2019) 118619. doi:10.1016/j.ijheatmasstransfer.2019.118619.

[41] N. S. Bondareva, N. S. Gibanov, M. A. Sheremet, Computational study of heat transfer inside different PCMs enhanced by al2o3 nanoparticles in a copper heat sink at high heat loads, Nanomaterials 10 (2) (2020) 284. doi:10.3390/nano10020284.

[42] R. S. Vajjha, D. K. Das, B. M. Mahagaonkar, Density measurement of different nanofluids and their comparison with theory, Petroleum Science and Technology 27 (6) (2009) 612–624. doi:10.1080/10916460701857714.

[43] T. Xiong, L. Zheng, K. W. Shah, Nano-enhanced phase change materials (NePCMs): A review of numerical simulations, Applied Thermal Engineering 178 (2020) 115492. doi:10.1016/j.applthermaleng.2020.115492.

[44] Z. Li, A. Shahsavar, A. A. Al-Rashed, P. Talebizadehsardari, Effect of porous medium and nanoparticles presences in a counter-current triple-tube composite porous/nano-PCM system, Applied Thermal Engineering 167 (2020) 114777. doi:10.1016/j.applthermaleng.2019.114777.

[45] H. I. Mohammed, P. Talebizadehsardari, J. M. Mahdi, A. Arshad, A. Sciacovelli, D. Giddings, Improved melting of latent heat storage via porous medium and uniform joule heat generation, Journal of Energy Storage 31 (2020) 101747. doi:10.1016/j.est.2020.101747.

[46] B. Leonard, A stable and accurate convective modelling procedure based on quadratic upstream interpolation, Computer Methods in Applied Mechanics and Engineering 19 (1) (1979) 59–98. doi:10.1016/0045-7825(79)90034-3.

[47] S. Patankar, Numerical heat transfer and fluid flow, Hemisphere Publishing Corporation; McGraw-Hill Book Company, New York., 2018.